18th Brazilian Congress of Thermal Sciences and Engineering
November 16-20, 2020 (Online)

ENC-2020-0091
THERMAL AND FLUID DYNAMICS SIMULATION OF A FLUIDIZED BED REACTOR FOR MRDF GASIFICATION

Vitor Alberto Lemes Monteiro
Maurício Guilherme Alves dos Reis
Cassius Ricardo Nascimento Ferreira
Universidade Federal de Uberlândia, Faculdade de Engenharia Mecânica, Av. João Naves de Ávila, 2121, 38408-100, Uberlândia-MG.
vitoralbertolemes@hotmail.com, mauricioalvesreis@gmail.com, cassiusferreira@gmail.com

Luciano Reis Infiesta
Carbogás Energia, Avenida Guaraciaba, 659, 09370-840, Mauá-SP.
luciano@carbogas.com.br

Solidônio Rodrigues de Carvalho
Universidade Federal de Uberlândia, Faculdade de Engenharia Mecânica, Av. João Naves de Ávila, 2121, 38408-100, Uberlândia-MG.
solidonio@ufu.br

Abstract. *Simulations of a fluidized bed reactor for gasification of municipal refuse-derived fuel (MRDF) from municipal solid waste (MSW) was performed using OpenFOAM software to investigate fluid dynamics of the fluidization behaviors. Experimental information was obtained from a gasification pilot plant located at Mauá-SP, Brazil, with capacity for 7.1 t day^{-1} of MRDF to produce 16.9 t day^{-1} of syngas. Eulerian-Eulerian modeling were applied and a gas-solid two-phase flow was considered to represent silica sand and gas in reactor. Thermophysical properties were calculated in function of operation temperatures and applied to energy transport equation, enclosing the energy balance. Air was used to represent all gaseous phases, which is insufflated at 673 K into the reactor maintained at 1123 K. The simulation results obtained shows the expected fluidizing characteristics for the pilot plant reactor.*

Keywords: *Eulerian-Eulerian, MSW, RDF, OpenFOAM, waste-to-energy*

1. INTRODUCTION

Many efforts have been done to minimize the waste generation among the growing consumption of the global population. Thus, the waste management includes from simpler techniques, like reuse and recycling, to complex methods like thermal and biological processing. In this context, the gasification stands out as a sustainable and renewable solution.

The gasification thermochemical process is worldwide applied for energy generation from coal and others homogeneous biomass. However, its use for energy recovering from heterogeneous biomass, such as waste, requires remarkable technologic knowledge. The main difficult of this research line is to apply this process on industrial scale projects, which demands many tests, experimentation and validation under the environmental laws and government support.

The academic community studies shows that the fluidized bed gasification has many advantages dealing with heterogeneous waste materials, such as uniformization of biomass and steady internal temperature. Therefore, the fluidization is widely studied to provide better performance of the reactors and more efficient energy conversion.

The author's group experimentally developed a fluidized bed reactor capable of recovering energy from municipal solid waste in large scale. Hereby, thermodynamics and mass balance information were gathered from its gasification pilot plant. Therefore, the main objective of this work is to study the fluid dynamics and the fluidization behavior of that semi-industrial scale gasification reactor for further developments.

2. EXPERIMENTAL INFORMATION

A fluidized bed gasification technology was developed by Carbogás Energia company on experimental basis over the years. Many tests were done to develop the current pilot plant located at the city of Mauá-SP, Brazil. The objective of this facility is to perform waste gasification tests in a large-scale reactor, different from those small-lab pilot plants reported

on literature. Such experimentation provided thermodynamic, mass and energy balance data, besides the equipment, design and operation information.

The gasification reactor is 9.975 m height and has 1.460 m of external diameter. Such equipment is capable of processing 296 kg h^{-1} of municipal refuse-derived fuel (MRDF) to produce 704.3 kg h^{-1} of syngas. Besides the biomass, the bed material consists of silica sand, limestone and the ash generated. The carbon steel reactor is thermally insulated. Internally, it also has a cyclone with helical channels at the upper part and a downdraft tube, which allows the separation of solids from gas without heat losses from the reactor. The extracted particles are returned to the bottom of the reactor and the product gas is released through the inner duct throughout the upper part of the system. Additionally, 79.96 kg h^{-1} of ash are constantly extracted of the bottom of the reactor.

Due to the waste gasification particularities, related to the its poor lower heating value (LHV), high moisture and varying particles size, our research group has developed a proper pretreatment for the municipal solid waste (MSW), described by Infiesta et al. (2019). Therefore, the authors preferred to use the nomenclature MRDF for the biomass used instead of the refuse-derived fuel (RDF) found in some works in literature, which is substantially different from the MRDF. The MRDF biomass has LHV of 14.6 ± 1.3 MJ kg^{-1}, moisture of 17 ± 8 wt.% and average particles size of 20 mm. Such features make the developed gasification process feasible.

Air is used as gasification agent, insufflated into the bottom of the reactor at 673 K (400 °C) to carry up all the materials inside at inlet pressure of 130 kPa and mass flow rate of 488.4 kg h^{-1}. The reactor operates at a uniform temperature of 1123 K (850 °C). The outlet measured pressure of the produced gas was slightly above atmospheric pressure.

3. METHODOLOGY

The OpenFOAM 8 software was used to simulate the reactor and results analyzed by ParaView software.

To simulate the internal fluid dynamics of the gasifier, the bed material was simplified and represented by one solid phase with the characteristics of the silica sand, with specific mass of 1,660 kg m^{-3} and particles diameter of 0.5 mm. The gas phase was represented by air, insufflated into the reactor at 673 K. At this work, the MRDF particles was not considered as well as the chemical reactions of the gasification process. Thus, a two-phase modeling was developed to concern the continuous gases phase and solid particle dispersed phase.

A Eulerian-Eulerian approach was implemented to handle both continuous and dispersed phases, once the greatest advantage of this method is the computationally efficient among others. Despite the limitations attaching chemical reactions, large number of particles and troubles in modeling flows with a range of different particle types and sizes, for example, good fluid dynamics simulation results are obtained from this modeling approach (Zhong et al., 2016). The mathematical equations of this method are presented by Rusche (2002). The energy and momentum transfer between the solid and gaseous phase were considered in this model using, respectively, the empirical correlation of Ranz-Marshall (1952) and Gidaspow model (1994). Reynolds-averaged Navier-Stokes (RANS) was implemented for turbulence closure equations. The kinetic theory of granular flows, proposed by van Wachem (2000), was used to evaluate the constitutive properties of the dispersed phase, and the gas-phase behavior was simulated employing the k-ε turbulent model. Thermophysical properties were calculated using Sutherland's Law (1893) and JANAF Thermochemical Tables (Chase, 1998).

3.1 Governing equations

The Eulerian-Eulerian approach solves the governing equations for each phase, in this case the gas media as the air and solid phase as silica sand. The sum of the volumetric particle fraction of the different phases is always unit. Those equations were properly detailed at Rusche's work (2002) and only the basic governing equations will be presented.

The continuity equation reads

$$\frac{\partial}{\partial t}\alpha_k\rho_k + \frac{\partial}{\partial x_i}\alpha_k\rho_k U_k = \dot{m}_k \tag{1}$$

The momentum equation reads

$$\frac{\partial}{\partial t}(\alpha_k\rho_k U_k) + \nabla\cdot(\alpha_k\rho_k U_k U_k) = \alpha_k\rho_k g_i + \nabla\cdot S_k + I_k \tag{2}$$

$$S_k = \nabla\cdot(\alpha_k\tau_k) - \alpha_k\nabla p - \nabla p_k \tag{3}$$

$$\tau_k = \mu_{eff}\frac{1}{2}\left[\nabla U_k + \nabla U_k^T\right] + \left(\lambda_k - \frac{2}{3}\mu_{eff}\right)(\nabla\cdot U_k)I \tag{4}$$

Energy transport equation

$$\frac{\partial}{\partial t}(\alpha_k \rho_k E_i) + \nabla \cdot (\alpha_k \rho_k U_k E_i) = \alpha_k \left(\frac{\partial p}{\partial t} + U_k \cdot \nabla p\right) - \nabla\left(\alpha_k k_{eff} \nabla T_k\right) + \phi + A_{sp} h (T^* - T_k) + \dot{q}_k \quad (5)$$

The index k is symbolic for the solid and the fluid phase, e.g. the particle solid phase fraction (α) may be denoted by α_p, the one of the gas continuous phases as α_g. At such equations, α_k is the volume fraction, ρ_k the density and U_k the velocity of the respective phase. The continuity equation show $\dot{m}_k$, which is the mass source term.

The momentum equation defines S_k as the *k*-phase stress tensor, p the pressure, p_k the granular pressure when solid phase, λ_k the solid bulk viscosity and I_k is the momentum exchange term which may include drag forces, turbulent dispersion, etc..

k_{eff} e μ_{eff} represents the effective thermal conductive and viscosity, which also includes the turbulent effects.

At the energy transport equation, ϕ is the viscous dissipation and E_i the enthalpy, $\dot{q}$ the heat source term, A_{sp} is the superficial area of the particle phase and T^* is the temperature of the exchange phase.

The drag model is written as a combination of the Ergun Equation (Ergun, 1952) and Wen and Yu drag model. The drag factor is the drag factor for a spherical particle given by (Schiller and Naumann, 1935). The combination of the two drag models leads to Gidaspow's Drag Model (Gidaspow, 1994). The Gidaspow's Drag Model is recommended for dense particulate flow, typical of this type of reactor (Zhong et al., 2016).

Empirical correlation used for calculating the Nusselt's number (Ranz-Marshall, 1952) to the heat flux between phases:

$$Nu = 2 + 0.6 Re^{0.5} \mathrm{Pr}^{0.33} \quad (6)$$

$$Nu = \frac{h d_p}{k} \quad (7)$$

The Sutherlands's transport modeling (Sutherlands, 1893) concerns evaluating dynamic viscosity (μ) in function of temperature from specific coefficient (A_s) and Sutherland Temperature (T_s) by the correlation:

$$\mu = \frac{A_s \sqrt{T}}{1 + \frac{T_s}{T}} \quad (8)$$

JANAF Thermochemical Tables (Chase, 1998) provides the coefficients of a polynomial relation to calculate the specific heat (c_p) as function of temperature (T).

The imposed velocity of the insufflated air to the bottom of the reactor can be defined as an interstitial velocity (U_i) or superficial velocity (U_s). The interstitial velocity is the average velocity that prevails in the pores of the column. Whereas, the superficial velocity is the quotient between the volumetric flow rate of the fluid and the cross-sectional area of the reactor bed (Perry et al., 1997). The relation of them is related the void fraction of the bed (ε), or simply α_{air} parameter of the simulations, as

$$U_i = \frac{U_s}{\varepsilon} \quad (9)$$

3.2 Meshing and Simulation settings

In order to validate the numerical system of the solver and analyze the consistency of results in terms of minimum fluidization velocity (U_{mf}), some simulations using the same numerical modeling were performed. This velocity is the most important measurement needed for design and determines the approximate limit between a fixed bed and a fluidized bed reactor. Therefore, a regular geometry and mesh was set accordingly the work of Shao et al. (2019) to investigate the pressure drop as function of the velocity of the air insufflated into the inlet of reactor.

For the pilot plant gasifier simulation, the geometry dimensions follow the experimental design, described at Section 2, which is shown in Fig. 1. Due to the high velocities, the turbulent phenomena assume an essential role at the fluid flow. Therefore, a 3D mesh was adopted for the obtention of physically realistic results, which are less sensitive to numerical issues (Shi et al., 2019). The geometry was designed and meshed with *snappyHexMesh* utility from OpenFOAM software. This way, the hexahedral cells meshing system was created to simulate half of the reactor, as shown in the Fig. 2, which shows also the boundary conditions selection, besides the symmetry longitudinal plane. The mesh is composed of 61,744 hexahedral cells and some prisms cells due small edges adjust, but all mesh regions have the same degree of refinement.

In this work, the outlet boundary adopted is the annular circle of entrance of the reactor's cyclone (Fig. 2), which was not added to geometry by means of simplification, once the main objective of this work is to investigate the fluidizing pattern of the bed. Furthermore, the simulation of this component would require better refinement of its cells, due to the high velocity caused by the section area reduction flow.

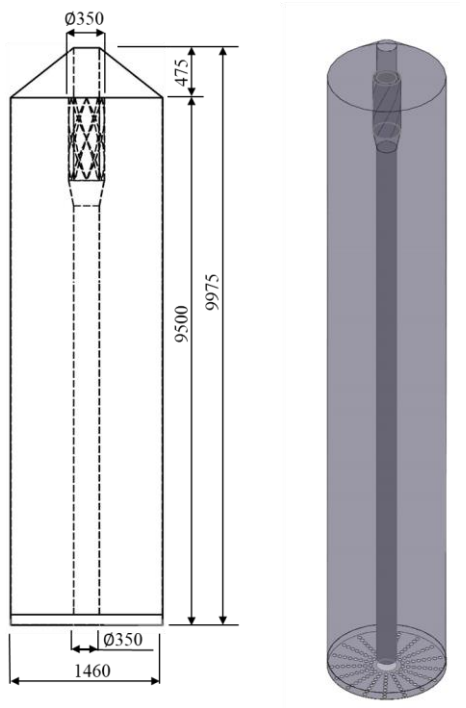

Figure 1. Geometry dimensions in millimeters and 3D design of the gasifier.

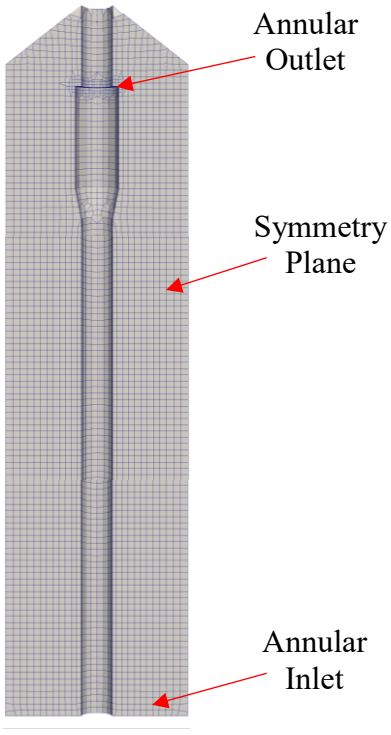

Figure 2. Meshing layout and boundary conditions.

The initial conditions used at the simulations, such as air inlet pressure and velocity, were adopted as the experimental reactor. Table 1 indicates the type of boundary conditions adopted. At all faces of the wall of the reactor was implemented a wall function of boundary condition, as shown at Tab. 1. Table 2 and Fig. 3 resumes the simulation parameters.

To estimate the amount of silica sand initially contained in the reactor, an arbitrary amount of sand was imposed to the model and the inlet pressure obtained by simulation. The particles mass was adjusted to reach the inlet pressure of the pilot plant reactor. The inlet air velocity was determined by the conversion of 488.4 kg h^{-1} to volumetric flow rate of

0.203 m^3 s^{-1} of hot air through the inlet surface of reactor. Based on the inlet air mass flow rate of the pilot plant reactor, the calculated interstitial velocity for that condition of air flow rate was 0.12 m s^{-1}.

Table 1. Boundary conditions* assigned to OpenFOAM case.

Variable	Inlet	Outlet	Walls
alpha.air	Zero Gradient	Zero Gradient	Zero Gradient
alpha.particles	Zero Gradient	Zero Gradient	Zero Gradient
alphat.air	Calculated	Calculated	alphatWallFunction
alphat.particles	Calculated	Calculated	Calculated
epsilon.air	Fixed Value	inletOutlet	epsilonWallFunction
k.air	Fixed Value	inletOutlet	kqRWallFunction
nut.air	calculated	calculated	nutkWallFunction
nut.particles	calculated	calculated	calculated
p	calculated	calculated	calculated
p_rgh	fixedFluxPressure	prghPressure	fixedFluxPressure
T.air	fixedValue	inletOutlet	Zero Gradient
T.particles	Zero Gradient	inletOutlet	Zero Gradient
Theta.particles	Fixed Value	Zero Gradient	Zero Gradient
U.air	interstitialInletVelocity	pressureInletOutletVelocity	No Slip
U.particles	Fixed Value	Fixed Value	No Slip

* All boundary condition funttions from OpenFOAM can be consulted at the OpenFOAM User Guide, available.

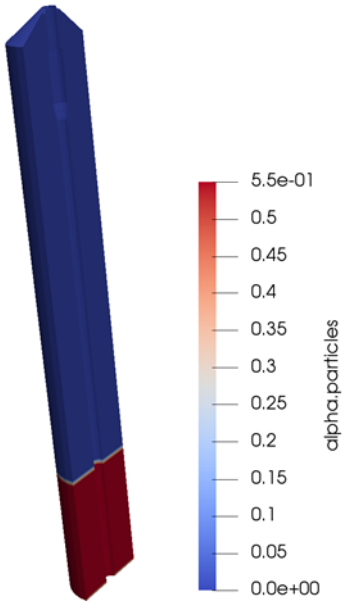

Figure 3. Initial condition of volumetric particle fraction.

Due to the absence of the MRDF biomass, which is not included into the simulated reactor by this moment, a constant mass source term ($\dot{m}_k$) was included to accomplish the mass balance of the reactor. Its value was calculated based on the mass flow rate of syngas production of 704.3 kg h^{-1} and air mass flow rate insufflated of 488.4 kg h^{-1}. Such calculation results in 107.95 kg h^{-1} of mass source term by the half of simulated reactor. Once the biomass and chemical reactions were not included to this modeling, the representative mass source term was uniformly distributed only to the region in which the particles are present. Thus, this parameter assumes nonzero value to all regions in which α_p is not null.

Table 2. Initial conditions and other Parameters.

Parameters	Value
Biomass feed rate (kg h^{-1})	N/A
Biomass temperature (ºC)	N/A
The density of biomass (kg m^{-3})	N/A
The density of bed material particles (kg m^{-3})	1,660
Bed material particles diameter (m)	0.5×10^{-3}
Temperature of air at inlet (ºC)	400
Interstitial velocity of air (m s^{-1})	0.0005 – 0.96
Temperature of fluidized gas (ºC)	850
Initial bed temperature (ºC)	850
Gasifier walls condition	Insulated
Inlet air volumetric flow rate (m^3 s^{-1})	0.203
Outlet pressure (kPa)	Atmospheric

4. RESULTS AND DISCUSSION

The comparison to a work of the literature is showed on Fig. 4, which a simplified geometry and mesh of fluidized bed system was simulated to verify the numerical modeling and results from the software. Shao et al. (2019) implemented the Eulerian-Lagrangian approach to simulate a fluidized bed reactor with silica and insufflated air. Results shows good correlation between results obtained by those authors and the present work.

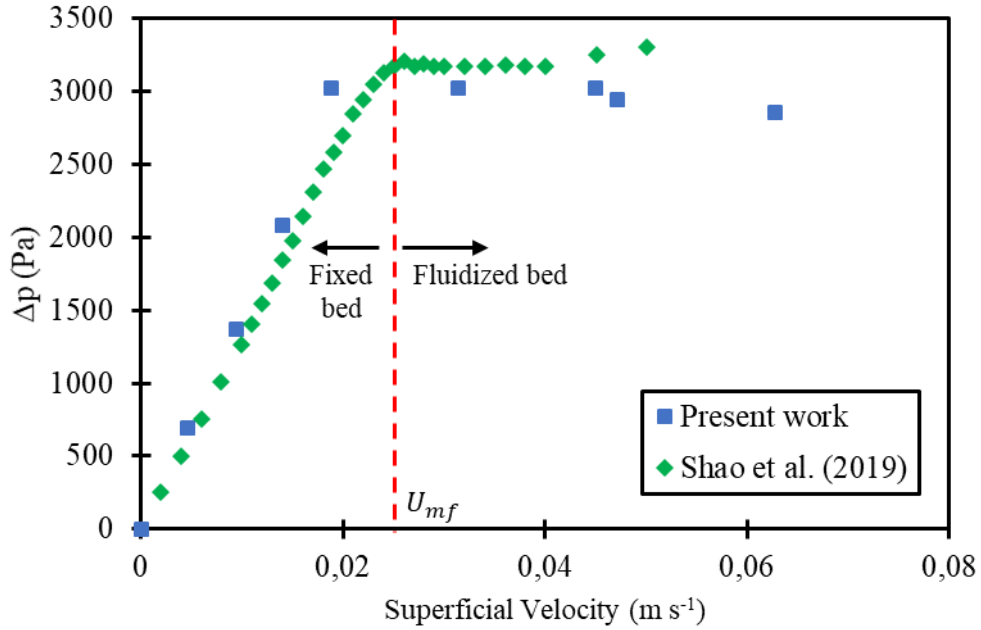

Figure 4. Correlation of the pressure drop as function of the superficial gas velocity.

Since the modeling seems to provide consistent results, the pilot plant reactor was configurated as the experimental pilot plant, described by the previous section. Mesh convergence is shown at Fig. 5, which the analyzed parameter was the pressure throughout the freeboard of the reactor (*z* coordinate). Almost linear profile of pressure was encountered at the bed region, mainly due to the drag forces caused by the sand particles of the bed and the pressure drop estimated value was almost 10 kPa m^{-1} as shown in the Fig. 5. The pressure drop profile was obtained due to the filling up with approximately 2,390 kg of sand to simulation. Fig. 5 also indicates that the mesh refinement degree is appropriate for the simulation, both in the bed region and above it.

Figure 6 shows the general aspect of bed fluidization with color scale in terms of volumetric particle fraction. The interstitial velocity varies from 0.0005 m s^{-1} to 0.96 m s^{-1}, which is possible to observe the main regimes of fluidization described by (Kunii and Levenspiel, 1991). As the velocity increases the smooth, bubbling fluidization and turbulent fluidization is observed as expected. The first regime (Fig. 6a) is a fixed bed condition, which is characterized by the highest volumetric particle fraction observed. The minimum superficial and interstitial velocity for the simulated pilot plant reactor encountered were 0,019 m s^{-1} and 0,004 m s^{-1}, respectively. Figure 6b the minimum fluidization regime is

observed, where the sand particles has reduced movement to form uniform porous bed. At Fig. 6c, occurs the smooth fluidization, despite of the dense particles and higher movement. Figure 6d may be a transition between smooth and bubbling fluidization, which can be better observed at Fig. 6e, where the bubbles are more recurrent. At Fig. 6f condition, the sand particles tend to be dragged above the bed and turbulent flow can increase gasification reaction rates.

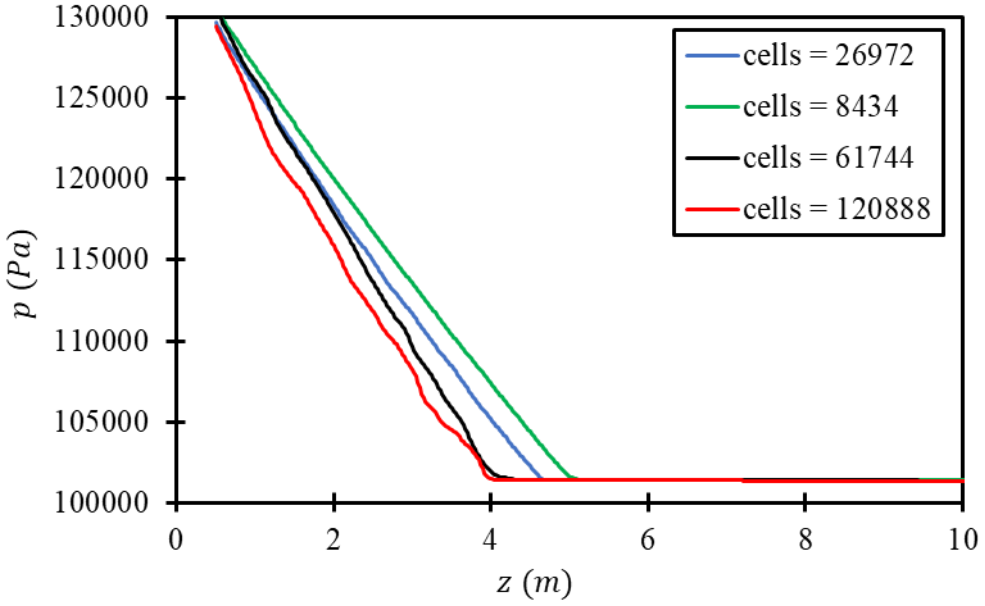

Figure 5. Pressure evaluated through z coordinate of reactor for mesh convergence.

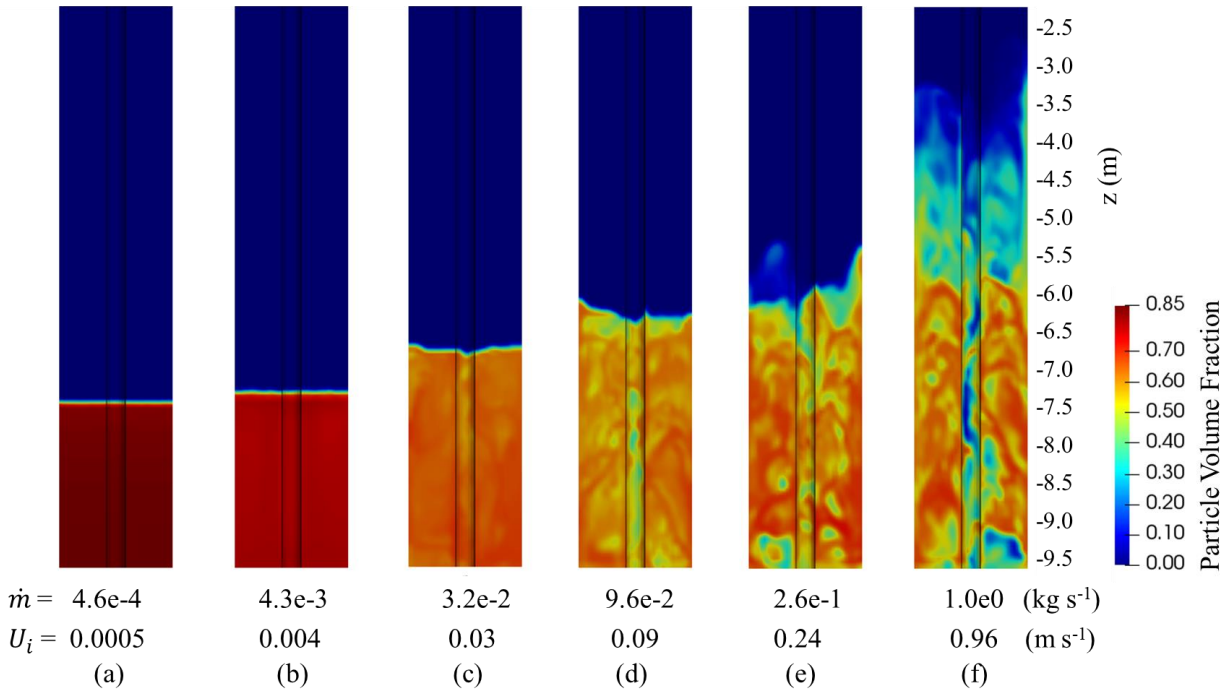

Figure 6. Regimes of Fluidization obtained for each air mass flow rate and interstitial velocity.

The interstitial velocity of inlet air for the continuous condition of operation of the reactor, as described at Section 2, is 0.12 m s^{-1}, which bubbling fluidized bed pattern expected. This velocity was set to the model and Fig. 7 shows the bed behavior. Highest speeds were observed at the bottom part of the reactor, whereas the upper part have similar velocities. This figure also shows the relative velocity between phase, which assumes higher values right above the bed interface. This may be explained by the expansion of the gas phase due to the constant mass source term adopted to represent the conversion of the MRDF solid biomass into gaseous products.

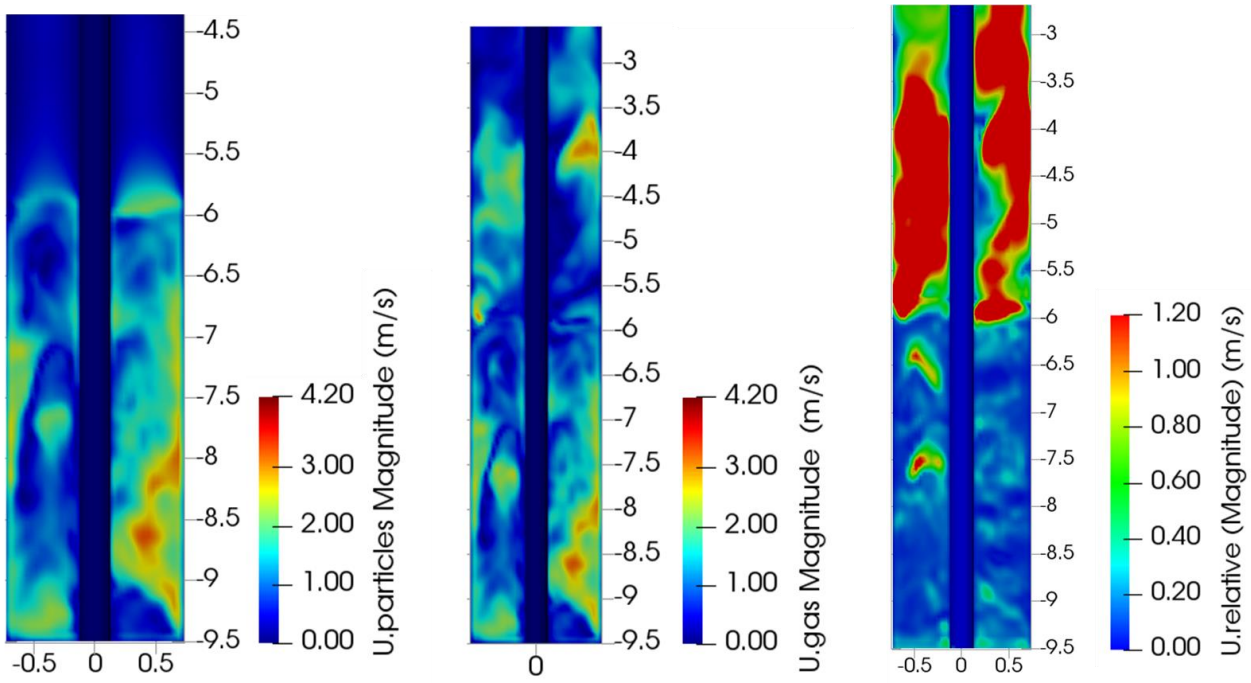

Figure 7. Velocities of particles, gas phase and relative velocity at the bed of reactor.

Figure 8 shows the pressure distribution of the reactor, which assumes the higher value at the inlet surface of the reactor but is gradually decreased throughout the bed region, as mentioned previously. The pressure drop at the middle and upper part of the reaction is negligible due to large diameter of the reactor, low drag forces and wall resistance.

According to Fig. 8, as the gas flow rises through the reactor, the formation of some air bubbles is observed due to the lower volumetric particle fraction values, where the gaseous phase starts to clump in an almost cohesive phase. At the upper part of the reactor, the bubbles acquire rounded shapes, scattered in the reactor. The distinction of some air bubbles maybe are not clearly showed because of the software image interpolation, which smooths the interface between air and sand particles. The grid of the mesh may also influence the final view of the fluidization pattern. The fluidization pattern exhibit particles uniformly distributed without the formation of large void spaces of air. This characteristic is suitable for the gasification reactions due to homogeneous heat distribution.

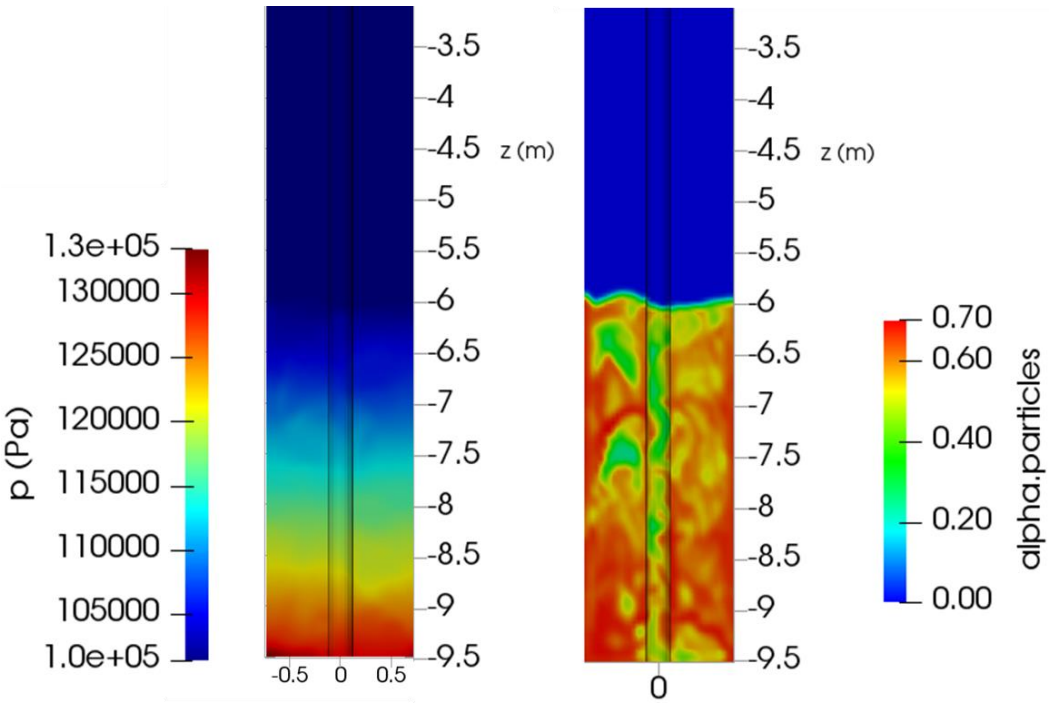

Figure 8. Pressure and volumetric particle fraction distribution throughout the reactor.

Figure 9 shows the results of some simulations performed to analyze the average inlet pressure and corresponding average volumetric particle fraction at inlet according to the air mass flow rate at different regimes of operation of the pilot plant reactor. The same pressure curve of Shao et al. (2019) and Kunii and Levenspiel (1991) is observed as expected. Once the mass flow rate is analyzed, the volumetric particle fraction is given at the inlet surface.

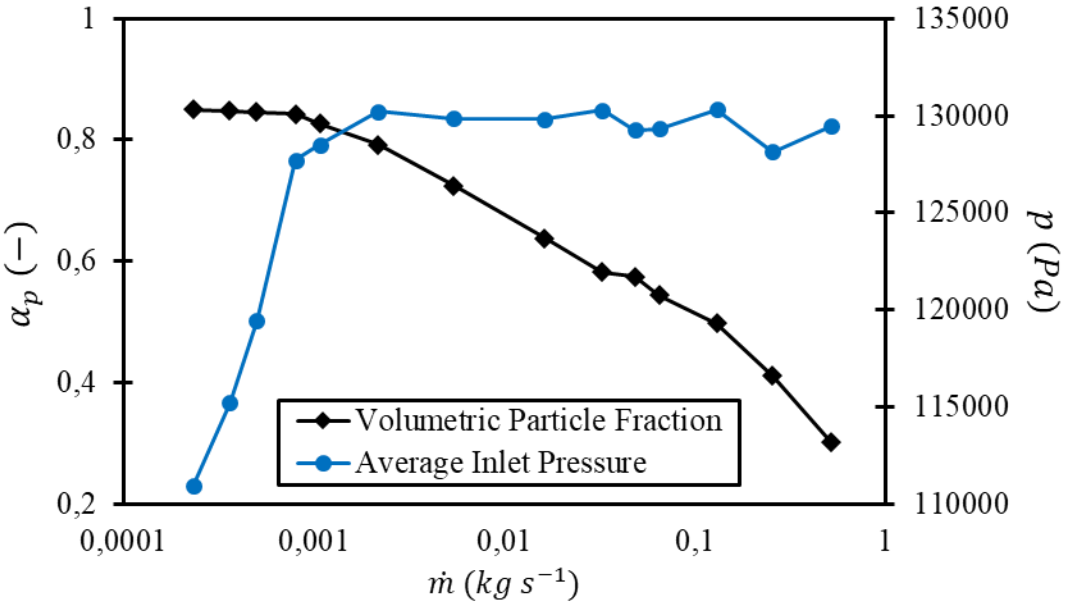

Figure 9. Volumetric particle fraction and average inlet pressure in function of air mass flow rate.

5. CONCLUSIONS

The energy recovery processing from waste is nowadays the most relevant research field of sustainable energy. In this context, the fluid dynamics simulations of this work aim to contribute to the renewable energy community. A semi-industrial scale MRDF gasification reactor was simulated to investigate the fluidization phenomena at the real operational conditions. Such results cooperate with the studies related to the municipal refuse-derived fuel of municipal solid waste.

The fluidization pattern obtained by the simulations were as expected for the experimental reactor of the pilot plant. The inlet air velocity and the bed movement behavior show that the fluidization regime is similar to a bubbling fluidized bed reactor. Furthermore, the simulations done in comparison with other works have led to consistent results with literature. Therefore, the fluidization modeling is able to provide important information to drive further studies and implementations.

6. ACKNOWLEDGEMENTS

The authors are grateful for the financial support provided by Furnas Centrais Elétricas S.A., Carbogás Energia Ltda., Agência Nacional de Energia Elétrica, Coordenação de Aperfeiçoamento de Pessoal de Nível Superior (CAPES), Conselho Nacional de Desenvolvimento Científico e Tecnológico (CNPq), and Fundação de Amparo à Pesquisa do Estado de Minas Gerais (FAPEMIG).

7. REFERENCES

Chase, M. W., 1998. *NIST-JANAF Thermochemical Tables*. National Institute of Standards and Technology (U.S.). 4th ed.

Ergun, S., 1952. “Fluid Flow through Packed Columns”. *Chemical Engineering Progress*., Vol. 48, pp. 89-94.

Gidaspow, D, 1994. *Multiphase Flow and Fluidization: Continuum and Kinetic Theory Descriptions*. Academic press, 1st edition.

Kunii, D. and Levenspiel, O., 1991. *Fluidization Engineering*. Series in chemical Engineering. Howard Brenner. Butterworth-Heinemann, 2nd edition.

Perry, R. H., Green, D. W., Maloney, J. O., 1997. *Perry’s Chemical Engineers’ Handbook*. McGraw-Hill. 7th Edition.

Ranz, W. E. and Marshall, W. R., 1952. “Evaporation from drops”. *Chemical Engineering Progress*, Vol. 48, pp. 141-146.

Rusche, H., 2002. “Computational fluid dynamics of dispersed two-phase flows at high phase fractions”. *Ph.D. thesis*, University of London, London, UK.

Schiller, L. and Naumann, Z., 1935. “A Drag Coefficient Correlation”. *Zeitschrift des Vereins Deutscher Ingenieure*, Vol. 77, pp. 318-320.

Shao, Y., Gu, J., Zhong, W., Yu, A., 2019. “Determination of minimum fluidization velocity in fluidized bed at elevated pressures and temperatures using CFD simulations”. *Powder Technology*. Vol. 350, pp. 81-90.

Shi, H., Komrakova, A., Nikrityuk, P., 2019. “Fluidized beds modeling: Validation of 2D and 3D simulations against experiments”. *Powder Technology*, Vol. 343, pp. 479–494.

Sutherland, W., 1893. “The Viscosity of Gases and Molecular Force”. *Philosophical Magazine*, Series 5, Vol. 36, pp. 507-531.

van Wachem, B. G. M., 2000. “Derivation, implementation, and validation of computer simulation models for gas-solid fluidized beds”. *Ph.D. thesis*, Delft University of Technology, Delft, Netherlands.

Wen, C. Y. and Y. H. Yu., 1966. “A generalized method for predicting the minimum fluidization velocity”. *AIChE Journal*, Vol. 12, pp. 610-612.

Zhong, W., Yu, A., Zhou, G., Xie, J., Zhang, H., 2016. “CFD simulation of dense particulate reaction system: Approaches, recent advances and applications”. *Chemical Engineering Science*, Vol. 140, pp. 16-43.

8. RESPONSIBILITY NOTICE

The authors are the only responsible for the printed material included in this paper.